Asymmetry between the electron- and hole-doped Mott transition in the periodic Anderson model

G. Sordi,[1] A. Amaricci,[1] and M. J. Rozenberg[1,2]
[1]*Laboratoire de Physique des Solides, CNRS-UMR8502, Université de Paris-Sud, Orsay 91405, France*
[2]*Departamento de Física, FCEN, Universidad de Buenos Aires, Ciudad Universitaria Pab. I, Buenos Aires 1428, Argentina*
(Received 13 February 2009; revised manuscript received 19 June 2009; published 27 July 2009)

We study the doping-driven Mott metal-insulator transition (MIT) in the periodic Anderson model set in the Mott-Hubbard regime. A striking asymmetry for electron- or hole-driven transitions is found. The electron-doped MIT at larger U is similar to the one found in the single band Hubbard model, with a first-order character due to coexistence of solutions. The hole-doped MIT, in contrast, is second order and can be described as the delocalization of Zhang-Rice singlets.

DOI: 10.1103/PhysRevB.80.035129 PACS number(s): 71.30.+h, 71.10.Fd, 71.27.+a

I. INTRODUCTION

The nature of the Mott transition, i.e., the metal-insulator transition (MIT) driven by electronic correlations, is a central problem in physics of strongly correlated electrons systems. The relevance of the problem was initially emphasized by Mott[1] in the 40s, trying to explain why some materials with odd electrons per the unit cell, such as NiO, are insulators. In a Mott MIT, a metallic system with a partially filled electron band suddenly opens an insulating gap. In practice the transition is usually driven by temperature, applied pressure, or chemical doping. The origin of the mechanism is in the correlation effects due to the strong on-site Coulomb repulsion experienced by electrons occupying rather localized orbitals, such as d in transition-metal oxides or f in heavy fermion compounds.

The classical example of an experimental system exhibiting a Mott transition is vanadium oxide V_2O_3, which has received continuous attention since the pioneering work of McWhan *et al.*[2] in the 70s. That compound has a finite temperature first-order metal-insulator transition that terminates at a high-temperature second-order critical point, in analogy with the finite liquid-gas transition line in water.

From a theoretical perspective, it is considered that the Hubbard model (HM), which contains a tight-binding band plus an interaction term that describes local Coulomb repulsion between electrons occupying the same site, is a minimal Hamiltonian that may capture the basic physics of the Mott MIT. The most significant work on this model was initiated by Hubbard[3] in the 60s, where, starting from the insulating state at large interaction values, he described how the system may close the correlation gap as the bandwidth is increased to values of the order of the Coulomb repulsion energy. Later, in the 70s Brinkman and Rice,[4] using a variational approach, started from the metallic state and showed how it can be destroyed by increasing correlation effects when the interaction strength becomes of the order of the bandwidth. Finally in the 90s the theoretical development of the dynamical mean-field theory (DMFT) (Refs. 5 and 6) allowed to get new insight on this problem. In the scenario for the Mott transition realized in the DMFT solution of the Hubbard model, for low temperatures and moderate interaction, the half-filled Mott insulator can be driven to a correlated metallic state through a *first-order* transition.[6] This transition can occur as a function of correlation strength, temperature, or doping. The solution of the Hubbard model within DMFT provided not only a connection between the approaches of Hubbard and Brinkman-Rice by showing how the system evolves from a metal to an insulator, but also produced a detailed description of the basic experimental phenomenology observed in the V_2O_3 compound.[6] In addition, it was later shown that the MIT can be described in terms of a Ginzburg-Landau scenario[7–9] with theoretical predictions for the critical behavior of observables near the second-order critical point that were eventually confirmed by experiments.[10]

The physics of the Mott transitions, especially those driven by doping at low temperatures, became of unparalleled interest in condensed matter physics with the discovery of the high-temperature cuprate superconductors[11] in the 80s and, in smaller but also significant measure, by the discovery of the non-Fermi-liquid behavior in heavy fermion systems.[12] In those systems, the effect of strong correlations is undisputed, since the active electronic degrees of freedom involve the localized d and f orbitals. Therefore, these systems are identified as doped Mott insulators, however, their phase diagrams and the evolution of their physical properties cannot be associated to the DMFT scenario for the Mott transition that was so successfully applied to V_2O_3.

Besides the Hubbard model, the periodic Anderson model (PAM) is another minimal Hamiltonian that is often investigated in the context of strongly correlated electron systems. That model contains two orbitals per unit cell, one local with on-site Coulomb repulsion and the other noninteracting and itinerant. At each lattice site, the two orbitals are hybridized. This model is more realistic than the Hubbard, since it describes with greater detail the actual situation in real compounds. For instance, in transition-metal oxides where the overlaps between neighboring oxygen p orbitals provide itineracy to the electrons, while the localized d orbitals of the transition metal experience the stronger correlation effects.

Despite the higher degree of detail included in the PAM, it is often assumed in theoretical approaches that the physical behavior of the PAM would result qualitatively similar to that of the Hubbard model at low frequencies. That statement can be mathematically justified in certain parameter regimes, however, its general validity is less evident

The DMFT is a theoretical approach that is mathematically exact in the limit of large lattice dimensionality[5,6] which has been extensively used to study the Mott transition in the Hubbard model, and, to a lesser degree, has also been employed to investigate the physics of the PAM.[13–16] Therefore, in the light of the previous discussion, a natural question to address is whether within DMFT the Mott transition scenario of the PAM is indeed qualitatively similar to that of the Hubbard model or, if contrary to usual expectations, it brings about new physical behaviors. This issue has been the focus of our recent investigations,[17] where we showed that in fact a different type of doping-driven Mott MIT is realized in the PAM, even in a parameter regime whether it might be expected that the identification with the Hubbard model may hold. The present study extends and provides further details to that work. In particular, we present data that illustrate the different behavior of physical quantities on the two sides of the transition, we provide comparisons of the Green's functions to results using a $T=0$ numerical technique, and we extend the discussion of the physical origin of two transitions. We should clarify that there is a qualitatively different insulator state that can be realized in the PAM, namely, the Kondo insulator. It is obtained in the particle-hole symmetric case, where the total occupation is *even* (i.e., two electrons per site). The Kondo insulator is qualitatively different from a Mott insulator, because it is due to band hybridization effect and correlations merely serve to reduce the hybridization gap. This insulator has a temperature-driven crossover to a metallic state that has been investigated within DMFT using quantum Monte Carlo (QMC) techniques.[18,19] In contrast, the Mott insulator state that we consider here corresponds to a state with *odd* total number of particles and its physical origin is entirely due to strong correlation effects.

The paper is organized as follows. In Sec. II we introduce the PAM and justify the choice of the parameter regime. We also summarize the DMFT equations and provide details on the numerical techniques we use to solve the associated impurity problem. In Sec. III we present the results and discuss the Mott transitions found in the PAM. In Sec. IV we present a discussion of the physical origin of the different scenario for the MIT found in the PAM with respect to the HM. In Sec. V we present the conclusions.

II. METHODOLOGY

A. Model

The Hamiltonian of the PAM is given by

$$H = -\sum_{\langle ij\rangle\sigma} t_{ij}(p^+_{i\sigma}p_{j\sigma} + p^+_{j\sigma}p_{i\sigma}) + (\epsilon_p - \mu)\sum_{i\sigma} p^+_{i\sigma}p_{i\sigma} + (\epsilon_d - \mu)\sum_{i\sigma} d^+_{i\sigma}d_{i\sigma} + t_{pd}\sum_{i\sigma}(d^+_{i\sigma}p_{i\sigma} + p^+_{i\sigma}d_{i\sigma}) + U\sum_i \left(n_{di\uparrow} - \frac{1}{2}\right)\left(n_{di\downarrow} - \frac{1}{2}\right). \quad (1)$$

Here $p_{i\sigma}$ and $p^+_{i\sigma}$ operators destroy and create electrons at p orbitals on site i with spin σ. The p orbitals have site energy ϵ_p and overlap via the hopping term $t_{ij}=t$ to form a band. $d_{i\sigma}$ and $d^+_{i\sigma}$ operators destroy and create electrons at d orbitals on site i with spin σ. The local d orbitals have site energy ϵ_d and are hybridized to the p orbitals with the constant on-site amplitude t_{pd}. U is the energy cost of double occupation of the d orbitals at each site and μ is the chemical potential. $\Delta_0 = \epsilon_d - \epsilon_p$, the difference between the d level and the center of the p band, defines the bare charge-transfer energy. Figure 1 shows a schematic representation of the Hamiltonian.

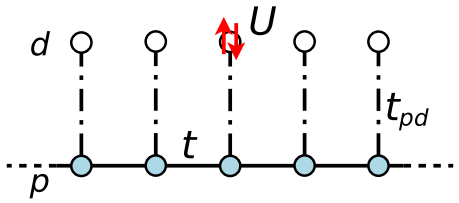

FIG. 1. (Color online) Schematic representation of the periodic Anderson model for the case of a one-dimensional chain. At each site of the lattice, a d orbital (open circle) hybridizes with a p orbital (full circle) through the amplitude t_{pd} (dot-dashed line). Two electrons in the d orbital experience a Coulomb repulsion U. The hopping amplitude between the p orbitals at neighboring sites i and j is $t_{ij}=t$ (solid line).

The insulator solutions of the PAM have been studied in literature mostly in the symmetric regime $\Delta_0=0$, $\mu=0$, where the system is a Kondo (or renormalized-band) insulator. In the present work, we shall focus on a different and less explored parameter regime, where the system is in a Mott insulator state. A key difference between these insulator states is that the former is realized at an even total electron occupation ($n_{\rm tot}=2$), while the latter is realized at an odd occupation ($n_{\rm tot}=1$ or $n_{\rm tot}=3$). Yet, the Mott insulator state may still be classified as a charge-transfer insulator or Mott-Hubbard insulator according to the Zaanen-Sawatzky-Allen scheme.[20]

The action associated with Hamiltonian (1) reads

$$S = -\sum_{k,\sigma}\int_0^\beta d\tau\int_0^\beta d\tau'\,\psi^+_{k\sigma}(\tau)\hat{G}^{-1}_{0\sigma}(\tau-\tau')\psi_{k\sigma}(\tau') + U\sum_i\int_0^\beta d\tau\left[n_{id\uparrow}(\tau) - \frac{1}{2}\right]\left[n_{id\downarrow}(\tau) - \frac{1}{2}\right], \quad (2)$$

where $\psi_{k\sigma}=\{d_\sigma, p_{k\sigma}\}$, $\psi^+_{k\sigma}=\{d^+_\sigma, p^+_{k\sigma}\}$, and the inverse matrix propagator $\hat{G}^{-1}_0$ is given by

$$\hat{G}^{-1}_{0\sigma}(k,i\omega_n) = \begin{pmatrix} i\omega_n + \mu - \epsilon_d & t_{pd} \\ t_{pd} & i\omega_n + \mu - \epsilon_p - \epsilon_k \end{pmatrix}, \quad (3)$$

where ϵ_k is the Fourier transform of the hopping term t. The lattice Green's function $\hat{G}$ is then written using the Dyson equation $\hat{G}^{-1}=\hat{G}^{-1}_0-\hat{\Sigma}$, where

$$\hat{\Sigma}_\sigma(k,i\omega_n) = \begin{pmatrix} \Sigma_\sigma(k,i\omega_n) & 0 \\ 0 & 0 \end{pmatrix} \quad (4)$$

and $\Sigma_\sigma(k,i\omega_n)$ is the d-electron self-energy. Here we are interested in a magnetically disordered state, thus the spin index can be dropped. In this case, the lattice Green's functions for the p and d electrons are explicitly given by

$$G_{pp}^{-1}(k,i\omega_n) = i\omega_n + \mu - \epsilon_p - \epsilon_k - \frac{t_{pd}^2}{i\omega_n + \mu - \epsilon_d - \Sigma(k,i\omega_n)}, \tag{5}$$

$$G_{dd}^{-1}(k,i\omega_n) = i\omega_n + \mu - \epsilon_d - \Sigma(k,i\omega_n) - \frac{t_{pd}^2}{i\omega_n + \mu - \epsilon_p - \epsilon_k}. \tag{6}$$

The local Green's functions are then obtained performing the integration over momenta,

$$G_\alpha(i\omega_n) = \frac{1}{N}\sum_k G_\alpha(k,i\omega_n) = \int \rho_0(\epsilon) G_\alpha(\epsilon,i\omega_n) d\epsilon, \tag{7}$$

where $\alpha = pp, dd$ and $\rho_0(\epsilon) = \Sigma_k \delta(\epsilon - \epsilon_k)$ is the free ($U=0$ and $t_{pd}=0$) density of states (DOS) of the p electrons.

The PAM has some simply solvable limits such as of vanishing hybridization, $t_{pd}=0$, or of vanishing correlation strength, $U=0$. For the latter case, the PAM describes two hybridized one-particle bands, which are obtained diagonalizing the Hamiltonian and read as

$$E_\pm(k) = \frac{1}{2}(\epsilon_d + \epsilon_p + \epsilon_k - 2\mu \pm \sqrt{(\epsilon_k - \Delta_0)^2 + 4t_{pd}^2}). \tag{8}$$

From the many interesting parameter regimes that this model has, we shall focus our study on a particular one where the low energy physics of the PAM is *a priori* expected to correspond to that of the Hubbard model. Thus, we consider the case where the localized d orbital is near the Fermi energy and with an occupation close to 1, while the p orbital band is well beneath in energy and almost fully occupied. By virtue of the hybridization term, the d electrons acquire a finite dispersion and form a narrow band that crosses the Fermi energy. It has a bandwidth $\sim t_{pd}^2/\Delta$, where Δ is the distance between the two hybridized bands, $\Delta \approx E_+ - E_- > \Delta_0$, and is subject to strong correlation effects when the on-site Coulomb term is turned on.

For reference, the solution for the noninteracting case in the chosen parameter regime is shown in Fig. 2. We set the units adopting a model semicircular density of states for the p electrons with half-bandwidth $D=2t=1$. As we shall see in the next section, this density of states is actually realized in a Bethe lattice in the limit of infinite spatial dimensions. In the upper panels we show the single particle dispersion $E_\pm$ and the resulting density of states for $\Delta_0=1$, $t_{pd}=0.9$, and $\mu=0.529$, which gives a total occupation per site $n_{\rm tot}$ equal to 3. In the lower panel we plot the total occupation $n_{\rm tot}=n_p+n_d$ together with the partial occupation. The plateaux in the curves signal incompressible states that correspond to insulators. These are observed at $n_{\rm tot}=2$ and $n_{\rm tot}=4$. In the first case, $n_{\rm tot}$ equal to 2, one has a hybridization gap insulator, since the band E_- is full and E_+ is empty. For $n_{\rm tot}=4$ the state is of a full band insulator. For $2<n_{\rm tot}<4$ the system is metallic, since the lower band with mostly p character is full and the narrow band with mainly d character is partially filled.

We shall now focus on the effects of correlation on such a metallic case, realized for $n_{\rm tot}=3$, where the lower electron band with mostly p character is close to being full (i.e., is occupied by two electrons) and the narrow d electron band is half-filled (i.e., with an occupation n_d close to 1). In the chosen parameter regime, there is a single band crossing the Fermi energy which has mostly d electron character. So correlations effects will affect it stronger. For values of the interaction U larger than its bandwidth $\sim t_{pd}^2/\Delta$ one may expect that a correlation gap would open and the system becomes a Mott insulator. This is the regime where the identification of the low energy physics of the PAM with the one-band Hubbard model may hold.

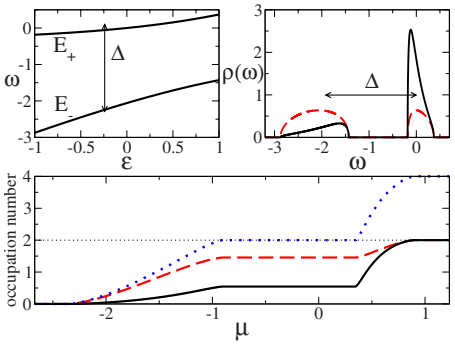

FIG. 2. (Color online) Top left panel: solid lines are the two branches $E_\pm(\epsilon)$ for $U=0$, $\Delta_0=1$, $t_{pd}=0.9$, and $\mu=0.529$, which gives $n_{\rm tot}=3$. Top right panel: density of states for the p and d electrons (dashed and solid lines) for the same model parameters as in the left panel. Note that the effective distance between the bands, $\Delta \approx 2$, results to be larger than the bare value $\Delta_0 = \epsilon_d - \epsilon_p = 1$. The free ($U=0$ and $t_{pd}=0$) DOS of the conduction electrons is semielliptical with a half-bandwidth equal to unity. Bottom panel: particle occupation n_d (solid line), n_p (dashed), and $n_{\rm tot}$ (dotted) as a function of the chemical potential for $U=0$, $\Delta_0=1$, and $t_{pd}=0.9$.

B. DMFT and the limit of infinite dimensions

To go beyond this qualitative discussion we need to obtain reliable solutions of the model Hamiltonian in the strongly interacting regime. We thus recur to the DMFT formulation where exact numerical methods can be used to solve the problem.[6]

The DMFT solution becomes exact in the limit of large spatial dimensionality[5] or, equivalently, large lattice connectivity z. For this limit to remain physical one is required to rescale the hopping t amplitude as $t/\sqrt{z}$, so that the density of states $\rho_0(\epsilon) = \Sigma_k \delta(\epsilon - \epsilon_k)$ gives a finite value for the mean kinetic energy.[5] As is well known in DMFT, the specific lattice structure is not essential and several lattice types could be used. For instance, the free (i.e., $t_{pd}=0$, $U=0$) density of states of the hypercubic lattice,[5,13] which is the generalization of the square lattice to the limit of high z, reads

$$\rho_0^{\rm hyper}(\epsilon) = \frac{1}{t\sqrt{\pi}} \exp\left(-\frac{\epsilon^2}{2t^2}\right), \tag{9}$$

where ϵ denotes the noninteracting single particle energy. Another lattice type which is often adopted is the Bethe lattice, whose density of states reads

$$\rho_0(\epsilon) = \frac{1}{2\pi t^2}\sqrt{4t^2 - \epsilon^2}. \quad (10)$$

In the following we shall adopt this type of lattice structure, as it is better suited for some of the numerical methods that we shall employ. As unit of energy we set the half-bandwidth of the Bethe lattice semicircular DOS, $D=2t=1$. The key mathematical simplification arising from the $z\to\infty$ limit is the locality of the self-energy, i.e., its k independence. Thus, there is no longer need to keep the momentum label in the single particle energies of the band structure ϵ_k, and the energy ϵ itself is simply kept as the quantum number.

C. Mean-field equations

In the limit of large lattice connectivity $z\to\infty$, the PAM can be exactly mapped onto a single impurity Anderson model supplemented with a self-consistency condition. The derivation of the DMFT equations has already been presented in detail elsewhere,[6,21,22] so here we shall just briefly summarize the main steps and the final expressions.

A direct way to derive the DMFT equations is to apply the cavity method.[6] The key idea is to focus on a given (any) site of the lattice and to integrate out the degrees of freedom on all the other lattice sites in order to obtain the local effective action at the selected site. In doing that, one shall also obtain a self-consistency condition which restores the translational invariance that was (temporarily) broken with the selection of a given lattice site. After integration of all sites other than the one selected, the local effective action is obtained,

$$S_{\text{eff}} = -\int_0^\beta d\tau \int_0^\beta d\tau' \sum_\sigma \psi_\sigma^+(\tau)\hat{\mathcal{G}}_0^{-1}(\tau-\tau')\psi_\sigma(\tau') + U\int_0^\beta d\tau \left[n_{d\uparrow}(\tau) - \frac{1}{2}\right]\left[n_{d\downarrow}(\tau) - \frac{1}{2}\right], \quad (11)$$

where $\psi_\sigma=\{d_\sigma,p_\sigma\}$ and $\psi_\sigma^+=\{d_\sigma^+,p_\sigma^+\}$ correspond to the two atomic orbitals of the given (arbitrary) site of the lattice. The local inverse propagator reads

$$\hat{\mathcal{G}}_0^{-1}(i\omega_n) = \begin{pmatrix} i\omega_n + \mu - \epsilon_d & t_{pd} \\ t_{pd} & i\omega_n + \mu - \epsilon_p - t^2\tilde{G}_{pp} \end{pmatrix}, \quad (12)$$

where $\tilde{G}_{pp}$ is the cavity Green's function that encodes the information of the propagation of electrons in the lattice, restricted not to return to the local site. These two equations define the so-called associated impurity problem of the model.

In order to restore the translational invariance and to obtain a closed set of equations, one has to relate the local inverse propagator $\mathcal{G}_0$ to the Green's function of the original lattice. In the Bethe lattice this relation is simple:[6] the p-electron cavity Green's function $\tilde{G}_{pp}$ becomes the local p-electron Green's function, $\tilde{G}_{pp}=G_{pp}$. From this relation and Eq. (12), one obtains the self-consistency condition for the impurity problem. It can be casted only in terms of $[\mathcal{G}_0]_{dd}$ and reads

$$[\mathcal{G}_0^{-1}]_{dd}(i\omega_n) = i\omega_n + \mu - \epsilon_d - \frac{t_{pd}^2}{i\omega_n + \mu - \epsilon_p - t^2 G_{pp}}. \quad (13)$$

In practice an iterative procedure is implemented to solve the set of DMFT equations: given an ansatz for $[\mathcal{G}_0]_{dd}$, and the fact that the interactions are local and only act on the d orbital, the impurity many-body problem (11) can be solved to produce a local d-electron Green's function $G_{dd}=-\langle dd^+\rangle_{S_{\text{eff}}}$. This defines a local self-energy $\Sigma=[\mathcal{G}_0^{-1}]_{dd}-G_{dd}^{-1}$ that allows for the calculation of the local p-electron Green's function G_{pp} [Eq. (7)],

$$G_{pp}(i\omega_n) = \int \frac{\rho_0(\epsilon)d\epsilon}{i\omega_n + \mu - \epsilon_p - \dfrac{t_{pd}^2}{i\omega_n + \mu - \epsilon_d - \Sigma(i\omega_n)} - \epsilon}. \quad (14)$$

The obtained G_{pp} and Σ are then used as input to the self-consistency condition Eq. (13) to produce a new $[\mathcal{G}_0]_{dd}$. This process is iterated until convergence is reached. *At the self-consistent point*, the Green's functions G_{dd} and G_{pp} and the self-energy Σ correspond to the local propagators of the original lattice model. Moreover, since in the $z\to\infty$ limit Σ is local, then all the k-dependent (or ϵ-dependent) propagators of the original lattice can also be computed from this self-energy.

It is useful rewrite the local Green's functions in terms of the Hilbert transform of the density of states $\tilde{D}(\xi)=\int_{-\infty}^{\infty} d\epsilon \rho_0(\epsilon)/(\xi-\epsilon)$. For the conduction electron Green's function G_{pp} we get

$$G_{pp}(i\omega_n) = \tilde{D}\left(i\omega_n + \mu - \epsilon_p - \frac{t_{pd}^2}{i\omega_n + \mu - \epsilon_d - \Sigma(i\omega_n)}\right) \quad (15)$$

and for the d-electron Green's function G_{dd} we obtain

$$G_{dd}(i\omega_n) = \frac{1}{i\omega_n + \mu - \epsilon_d - \Sigma(i\omega_n)} + \left[\frac{t_{pd}}{i\omega_n + \mu - \epsilon_d - \Sigma(i\omega_n)}\right]^2 G_{pp}(i\omega_n). \quad (16)$$

This expression has a transparent physical interpretation: there are two processes that a d-electron can undergo: either remain fluctuating at the local site (first term), or fluctuate for some time, then jump to the p site and propagate, and then return and fluctuate some more time (second term).

D. Numerical solution

For the solution of the associated impurity many-body problem (11), one may use a variety of techniques.[6] Here we shall employ two numerical methods which are both *a priori* exact: Hirsch-Fye QMC (Ref. 23) and exact diagonalization (ED). The interest of using different techniques is that they have complementary range of applicability and that they allow for a cross-check of the numerical results. The first

method, QMC, is a finite temperature calculation and is exact in the statistical sense. The other method is formulated at $T=0$ and relies on a finite-size representation of the local site environment (i.e., the cavity Green's function) by a bath of noninteracting atomic sites connected to the local impurity. In the limit of large number of atomic sites in the bath, this approach also becomes *a priori* exact. Both methods have already been well documented in the literature,[6] so here we shall limit ourselves to briefly provide the relevant technical details.

To implement the QMC, it is useful to first perform the integration on the noninteracting local p site in action (13), so that in the many-body problem the interacting d orbital is the only explicit degree of freedom. We then solve the impurity problem using the standard Hirsch-Fye QMC algorithm,[23] where the imaginary time interval $[0,\beta]$ is discretized in L time slices of width $\Delta\tau=\beta/L$ (where β is the inverse temperature). We set $U\Delta\tau<1$ to limit the systematic errors introduced by the Trotter decomposition. The precision of the calculations then basically depends on two remaining factors, the statistical error and the criterion for the convergence of the solution of the DMFT equations. For the former, we typically perform 10^5 sweeps. When required, we may do up to 10^6 sweeps, such as near the Mott transition, or to compute the analytic continuation of data to the real axis using the maximum entropy method.[24] The quality of the convergence is controlled by monitoring the behavior with iteration number of $G_{dd}(i\omega_1)$, the imaginary part of the d-electron Green's function at the first Matsubara frequency, which shows the largest variations. We stop the DMFT iterations when the fluctuations of this quantity become on the order of the QMC statistical error and remain stable for a few more iterations. In generic regions of the parameter space we have studied, the solutions converge in less than 20–30 iterations, but hundreds may be necessary close to a phase boundary.

The ED algorithm is based on the representation of the cavity Green's function by finite number auxiliary atomic sites.[6] They conform the "bath" or environment of the local impurity. In general, an infinite number of sites may be required to faithfully represent the dynamic environment; however, this is not possible to do in practice. Therefore, one has to adopt a strategy to best represent the environment with a finite number of auxiliary sites. One may use two different "geometries" to represent the bath: either the "chain" geometry, as described in Ref. 25 or the "star" geometry, as described in Refs. 26 and 27. In both cases, the effective impurity problem consists of a central impurity site, composed of an explicit d orbital and a p orbital, where, by virtue of Eq. (12) only the latter is connected to the bath. In practice, less than ten sites can be dealt with in this method and the ED is performed at $T=0$ using the Lanczos technique, which is convenient to obtain the Green's functions. In the case of the chain, parameters of the auxiliary atomic sites can be obtained in terms of a continued fraction expansion of the computed Green's functions.[6,25] On the other hand, in the case of the star geometry, the parameters are obtained by a χ^2 minimization of the difference between the computed local Green's function and a finite-size parametrization of the cavity.[6,26]

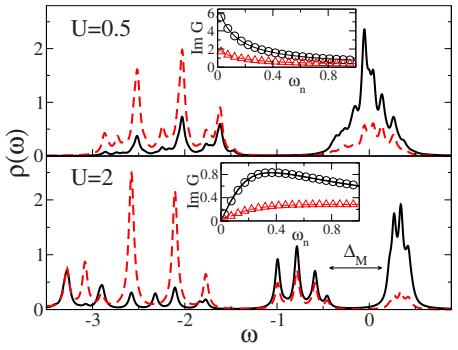

FIG. 3. (Color online) Density of states for the p and d electrons (dashed and solid lines) as obtained from ED-DMRG calculations (with a 40-site chain) at $\Delta_0=1$, $t_{pd}=0.9$, and $n_{\rm tot}\approx 3$. Top panel has $U=0.5$ and $\mu=0.612$. Bottom panel has $U=2$ and $\mu=1.029$. The arrow indicates the width of the Mott gap $\Delta_{\rm M}$. Insets: imaginary part of the p- and d-electron Green's functions. Data are from QMC at $T=1/128$ (open symbols) and ED-DMRG (lines). The finite (zero) value at $\omega_n\to 0$ shows the metallic (insulating) character of the solution at $U=0.5$ $(U=2)$.

The ED method can be substantially improved by supplementing it with the density-matrix renormalization group (DMRG) technique.[28–30] Several ED-DMRG procedures for the solution of the DMFT equations have been proposed recently.[28,30–32] The ED-DMRG method that we use here is in essence identical to the ED with the linear chain.[31,33] Since the linear geometry is perfectly adapted for the DMRG procedure, we can "grow" the bath to contain a higher number of auxiliary sites with respect to the standard ED.[30] In practice, we use up to 40 sites. Nevertheless, we point out that despite the large number of sites the spectral functions on the real frequency axis do not become continuous but still show a discrete multipole structure. We also observe that the number of poles is roughly similar to the number of sites, but the spectral weight remains rather concentrated in a relatively small number of poles, emphasizing the discrete nature of the Green's functions. However, this does not prevent that the agreement on the Matsubara imaginary frequency axis is usually excellent (e.g., see Fig. 3).

III. RESULTS

A. Mott insulating state

In this section we shall present our results for the Mott-Hubbard regime. In the Hubbard model, the system undergoes a Mott metal-insulator transition when the density is $n=1$ and the interaction strength U becomes of the order of the bandwidth.[6] Here, a similar phenomenon is expected as U is increased to a value of the order of the effective bandwidth at the Fermi energy $\sim t_{pd}^2/\Delta$ and keeping n_d at about 1. As described before, the Mott state is realized by setting a value of the interaction larger than the effective bandwidth $U>t_{pd}^2/\Delta$ and keeping the total occupation $n_{\rm tot}=n_p+n_d=3$. Similarly to the Hubbard model case, in the PAM there is an on-site Coulomb interaction acting on d orbitals. This interaction punishes the double occupation of d sites and conse-

quently favors the tendency to localization and to magnetic moment formation of the d electrons.

Notice that we have chosen in the definition of our Hamiltonian (1) and Eq. (11) the so-called nonmagnetic form for the interaction. This is motivated by the fact that we are interested in the Mott physics of a paramagnetic correlated state at $n_d \approx 1$, i.e., $n_{d\uparrow}=n_{d\downarrow}\sim 1/2$. Therefore the interaction term $U(n_{d\uparrow}-\frac{1}{2})(n_{d\downarrow}-\frac{1}{2})$ approximately cancels at the Hartree-Fock level. This allows to obtain some immediate physical insight. The cancellation implies that for low values of U, where first-order perturbation holds, the interacting density of states of the model remains essentially identical as in the noninteracting case (see Fig. 2, upper panels). Therefore, the position of the correlated narrow band remains approximately fixed at the Fermi energy. Since the position remains unrenormalized, at higher values of U one would expect that the narrow band splits, forming a lower Hubbard band and an upper Hubbard band, below and above the Fermi energy, respectively, and both carrying half of the spectral intensity of the narrow band. At the Fermi energy a large charge gap would then open and the system becomes a Mott insulator.

1. Opening of the Mott gap

This scenario is in fact borne out in the actual model solution that is shown in Fig. 3. The data correspond to a $T=0$ calculation using the ED-DMRG method with 40 sites in the bath. The values of the interaction are $U=0.5$ (upper panel) and $U=2$ (lower panel). This latter value of U is sufficient to drive the system to the Mott insulating state. In fact one may estimate that the critical U should be about twice the effective bandwidth t_{pd}^2/Δ (we shall present later on the full phase diagram). The insets of the figure contain a comparison of the results for the Green's functions in Matsubara frequency from ED-DMRG at $T=0$ and QMC at the low temperature $T=1/128$. The agreement is very satisfactory. The ED-DMRG method also provides the propagators in real frequency; we thus plot the more intuitive DOS in the main panels of the figure. In the weakly correlated case (upper panel), the DOS resembles the noninteracting one: at lower energies $-3 \lesssim \omega \lesssim -1.5$ there is a band with dominant p character, while at the Fermi energy there is a narrower band with mainly d character. In the Mott insulating state shown in the lower panel, the DOS consists of three features: similarly as before, there is a p-like band at high (negative) energies. However, the main qualitative difference is that now the narrow band at E_F is split in a lower Hubbard band and an upper Hubbard band, respectively, below and above the Fermi energy. The Mott-Hubbard character of the transition in this parameter regime is seen from the fact that both lower and upper Hubbard bands have dominant d character. Moreover, one also observes that the p component is not negligible, especially in the lower Hubbard band.

We should also mention that the apparent multiple peak structure of the main three features appearing in the DOS is merely due to the discreteness of the finite number of sites used to describe the environment in the ED technique. Though we are using as many as 40 auxiliary sites in the environment, the discretization effect still remains rather noticeable. Nevertheless, the splitting of the narrow band at the Fermi energy with the consequent opening of a large Mott gap Δ_M that signals the Mott insulator state is clearly observed.

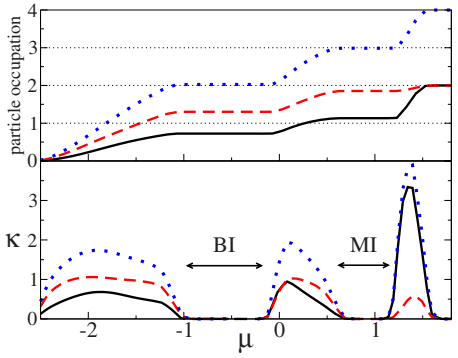

FIG. 4. (Color online) Top panel: n_d (solid line), n_p (dashed line), and $n_{\rm tot}$ (dotted line) as a function of the chemical potential μ for $U=2$. Data are from QMC calculations at $\Delta_0=1$, $t_{pd}=0.9$, and $T=1/64$. A large Mott gap opens at $U=2$ around $0.7 \lesssim \mu \lesssim 1.2$. Bottom panel: charge compressibility, $\kappa=\partial n/\partial\mu$ versus μ for the same model parameter as in the top panel.

The transition from metallic to insulating state with the consequent opening of the Mott gap can be also observed from the behavior of the partial p, d, and total particle occupation n_p, n_d, and $n_{\rm tot}$, respectively, as a function of the chemical potential. In Fig. 4 we show these quantities and their first derivative $\kappa=\partial n/\partial\mu$ proportional to the charge compressibility, for $U=2$. The plateaux observed in the occupations, with the respective vanishing of the compressibility for $n_{\rm tot}=0$ and $n_{\rm tot}=4$, correspond to the completely empty or completely full band insulators. The case $n_{\rm tot}=2$ corresponds to the hybridization band insulator, similar to the one already discussed in the noninteracting case. However, in contrast to the results for the noninteracting case, the strong value of the interaction creates additional plateaux in the $n(\mu)$ curves. The new plateaux occur when the total number of particles is exactly $n_{\rm tot}=3$, which is odd and signals the Mott state.

An important aspect that we should mention is that the Mott insulator state occurs where the correlated d site has an occupation close to 1, but not exactly unity. This can be seen is Fig. 4 (top panel), where the Mott plateau occurs at $n_d=1+\nu$ (and $n_p=2-\nu$), with $\nu \approx 0.13$. The specific value of ν depends on the hybridization and therefore one can consider it as a measure of the mix-valence character of the Mott insulating state. It is the *total* number of particles exactly equal to three (or one hole) what is required for the onset of the Mott insulator state. This implies that in this model where the mixed $p-d$ valence is explicitly included through the hybridization, the Mott localization occurs for a "composite" object which has a mixed p and d character.

2. Size of the Mott gap

The size of the Mott gap is naively expected of be of order U since it should mostly reflect the energetic cost to doubly occupy the d orbitals. However our results show that the size of the Mott gap Δ_M may be substantially smaller

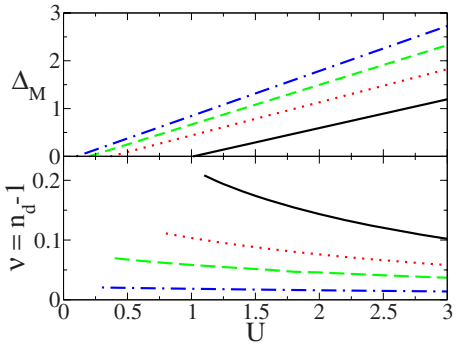

FIG. 5. (Color online) Top panel: size of the Mott gap Δ_M as a function of U for different positions of the p-electron band $\epsilon_p = -6, -3, -2, -1$ (top to bottom). Lower panel: mix-valence character $\nu = n_d - 1$ as a function of U for the same position of the p band as in the upper panel (bottom to top). The results are obtained from ED.

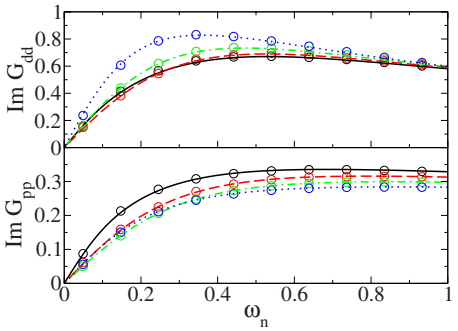

FIG. 6. (Color online) Top panel: imaginary part of the d-electron Green's functions in the Mott state, from ED-DMRG (for a large finite cluster of 30 sites) at $T=0$ and $\mu = 0.729, 0.829, 0.929, 1.029$ (solid, dashed, dotted-dashed, and dotted lines, respectively). Circles are the same quantity from QMC at $T=1/64$. Lower panel: imaginary part of the p-electron Green's functions; all model parameters are the same as in the top panel.

than the bare value U. In Fig. 5 we plot Δ_M as a function of U, for several values of the bare position of the p-band ϵ_p, which amount to increase the charge-transfer energy Δ_0. As the energy of the p orbitals is shifted down to larger (negative) energies, the effective bandwidth of the narrow band at the Fermi energy decreases. In addition, the p-electron band becomes essentially full with $n_p \to 2$ as $\epsilon_p \to -\infty$ (and keeping t_{pd} fixed). This implies a decrease in the mix-valence character of the electrons at the Fermi energy ν as shown in the lower panel of Fig. 5. In this limit the size of the Mott gap approaches the "bare" value $\Delta_M \approx U$. However, it is interesting to observe that the smaller values of ϵ_p lead to a substantial renormalization of the size of the expected Mott gap. This effect can be thought as due to an effective screening that the p electrons provide, or, in more naive terms, because the electrons only "feel" the repulsive term U during the time they spend on the d orbital, but not when they visit the p site. So as the mixed $p-d$ character is increased, the effect of the U is renormalized downward.

For completeness we show the behavior of the imaginary part of the Green's functions at low Matsubara frequency. In Fig. 6 we present numerical results for several insulating states obtained varying the chemical potential within the Mott plateau. The data were obtained with both QMC and ED-DMRG, so also serve to illustrate the good agreement between the two methods. Note that the imaginary part of both the p- and the d-electron Green's functions goes to zero at $\omega_n \to 0$. By analytic continuation this implies that the p- and d-electron DOS vanish at the Fermi level, consistent with the insulating character of the solutions. Accordingly, when the chemical potential μ is varied within the Mott plateau, the p- and d-electron DOS simply experience a rigid shift in energy. However, as we shall see later, there are dramatic changes in the DOS line shapes as the system turns metallic upon doping.

B. Doped Mott insulator

So far we have shown that the model does have a Mott insulator state which similarly as in the Hubbard model case develops two incoherent Hubbard bands above and below the Fermi energy. However, unlike in the Hubbard model case, the size of the gap, i.e., the separation between the Hubbard bands, may be substantially smaller than U if the hybridization is relatively high. In the following section we shall proceed to dope this Mott insulator with δ carriers, with $\delta = n_{\rm tot} - 3$. As was already reported in Ref. 17, we will observe that the insulator to metal transitions that can be obtained by either particle, $\delta > 0$, or hole doping, $\delta < 0$, are qualitatively different. The former will essentially reproduce the known scenario for the Mott MIT that is realized in the DMFT solution of one-band Hubbard model.[6,33–35] This was to be expected since we have tuned the parameters of the model to the regime where the identification of the low energy physics of the PAM and the one-band Hubbard model was expected to hold.[36] However we shall see that, rather surprisingly, the hole doping insulator to metal transition bears out a qualitatively different scenario.

1. Particle doping ($\delta > 0$)

In this section we shall first describe the MIT driven by particle doping and demonstrate that it realizes the same first-order transition scenario as the one in the single band Hubbard model. The metallization of the Mott insulator is most directly seen from the changes that take place in the density of states. In Fig. 7 we show the evolution of that quantity for the p- and d-electron components as a function of doping. The data are obtained from analytical continuation of QMC results at $U=2$ and low temperature. To compute the analytical continuation using the MEM, we used over 10^6 sweeps, so to minimize the uncertainty due to statistical errors. In the left top panel we see the DOS for the case where the chemical potential μ is close to the upper energy edge of the Mott gap, therefore still in the insulator state with $\delta = 0$. The left bottom panel shows the metallic state that is obtained when the chemical potential enters the upper Hubbard band, doping the parent Mott insulator with particles. We observe a broad peak at the Fermi energy and a strong transfer of spectral weight from the lower to the upper Hubbard

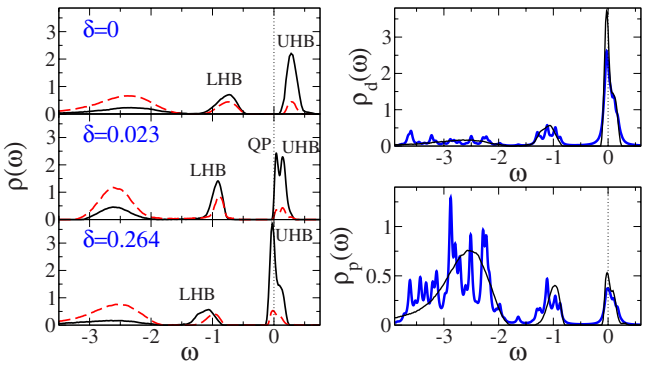

FIG. 7. (Color online) Density of states for the p and d electrons (dashed and solid lines) at $U=2$, $\Delta_0=1$, and $t_{pd}=0.9$. Left: DOS from analytically continued QMC data at $T=1/64$. Top panel has $\mu=1.079$ corresponding to a Mott insulating state ($\delta=0$). Middle panel has $\mu=1.244$ corresponding to small doping $\delta=0.023$. Bottom panel has $\mu=1.317$ corresponding to high doping $\delta\approx0.26$. Right panels: comparison of DOS from ED-DMRG and QMC data (thick and thin lines, respectively) at $\delta=0.264$.

band. The d orbital character remains dominant in the DOS upon doping. In the left middle panel we show the DOS in the region of small doping, very near the transition. The data reveal that both the p- and d-electron components of the DOS show a narrow quasiparticle peak at the Fermi energy flanked by the incoherent upper Hubbard band at higher energies. This coherent peak carries a small fraction of the spectral intensity which is of order δ. In addition, from the enhancement of the slope of the self-energy, one observes that the quasiparticles acquire a heavy mass. All these features are consistent with the MIT scenario found in the one-band Hubbard model.

The right panels of Fig. 7 show a comparison of QMC and ED-DMRG results for the DOS at high doping. The discrete peaks in the ED-DMRG data are due to the finite number of sites in the effective bath. Nevertheless, the agreement in the distribution of the spectral weight of the two methods is very satisfactory. The comparison of the data also allows for a nontrivial benchmark of the numerical results and is a useful illustration of the advantages and disadvantages of the different numerical techniques. ED-DMRG is exact but has the drawback of discrete poles structures that persist even for many effective atoms in the bath. QMC, in contrast, produce smooth spectra but their numerical precision cannot be guaranteed due to the uncertainties in the process of analytic continuation of data to the real frequency axis.

In Fig. 8 we present the d-electron density of states $\rho_d(\omega)$ for several values of particle doping. The data show the presence of the quasiparticle peak evolving in between the two Hubbard bands. One may see that though the data show a reasonable systematic evolution some details are beyond the precision of the technique, such as the precise size of the gap and the form of the band edges.

The most substantial confirmation that the particle doping-driven MIT scenarios in the PAM and in the HM are in fact qualitatively analogous comes, however, from the observation of the hysteresis effect in the particle number $n(\mu)$

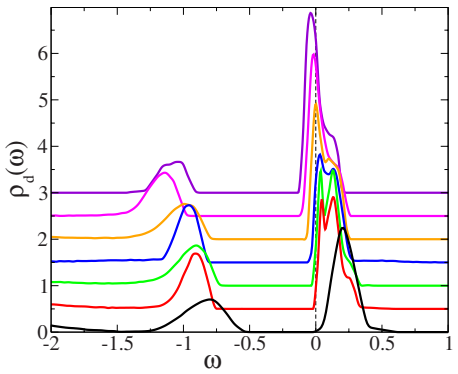

FIG. 8. (Color online) Density of states for the d electrons from QMC data at $U=2$, $\Delta_0=1$, $t_{pd}=0.9$, and $T=1/64$. The particle doping is $\delta=0$, 0.01, 0.02, 0.04, 0.11, 0.21, and 0.32 (bottom to top).

curve. The hysteresis is a hallmark of the first-order nature of this doping-driven transition and it was observed and studied in detail in the Hubbard model.[34,35,37–39] We also find it here in the PAM and it is most clearly appreciated in the behavior of n_d versus μ. There is a strong dependence of the $n_d(\mu)$ curves as the temperature is lowered signaling strong correlation effects being active with very low energies. In Fig. 9 we show the occupation of the d electrons as a function of the chemical potential μ obtained from QMC. The main panel shows a detail of the QMC data at the low temperature $T=1/64$, where the hysteresis loop can be clearly seen. These results were verified using the $T=0$ ED technique.

In order to observe the hysteresis cycle, we use as a seed for the iterative procedure the converged solution from the previous set of parameters.[34,37] Thus, the solutions can be continuously "followed" in parameter space, until it shows a sudden jump. The discontinuous jump occurs at the approximate position of the spinodal lines.[40] Similarly as in previous studies on the Hubbard model,[37] the hysteresis defines a region of parameters where two solutions of the DMFT equa-

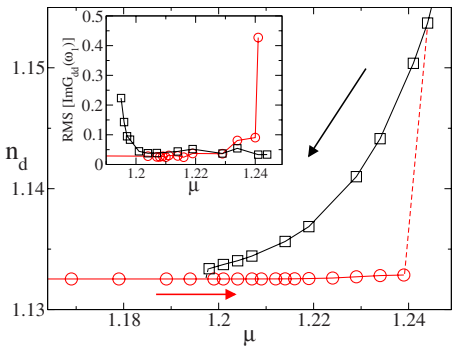

FIG. 9. (Color online) Hysteresis loop for the $n_d(\mu)$ curve at the upper energy edge of the Mott insulating state. Data are obtained from QMC for $T=1/64$ at $U=2$, $\Delta_0=1$, and $t_{pd}=0.9$. The arrows indicate the solution obtained by following the insulating (circles) and the metallic solution (squares). Inset: root mean square (rms) of the imaginary part of the d-electron Green's function value at the first Matsubara frequency as a function of the chemical potential. It shows the enhancement of the fluctuation near the two critical values of chemical potential, where the continued solution ceases to exist.

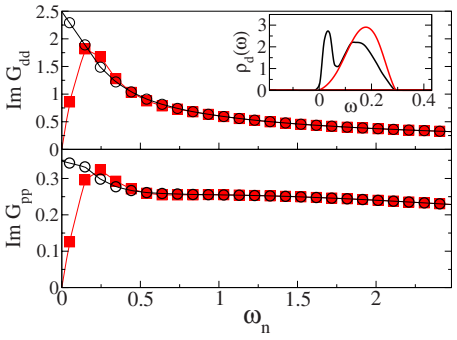

FIG. 10. (Color online) Main panel: imaginary part of the d-electrons Green's function as a function of the Matsubara frequency for $\Delta_0=1$, $t_{pd}=0.9$, $U=2$, $T=1/64$, and $\mu=1.234$ corresponding to tiny particle doping $\delta=n_{\rm tot}-3\approx 0.01$. Open symbols correspond to the metallic solution, while full symbols to the insulating one. Inset: the correspondent d-electron density of states $\rho_d(\omega)$. Thick line is the metallic solution; thin line is the insulating one.

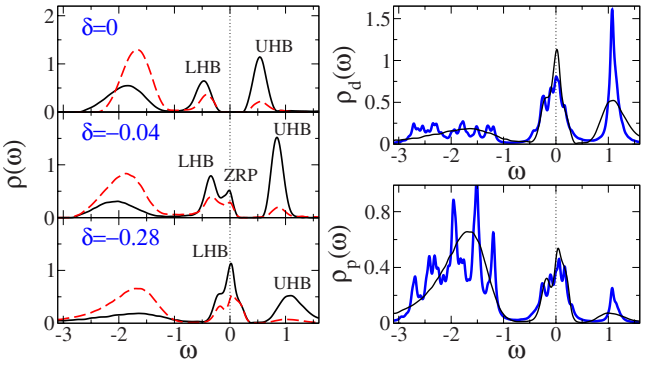

FIG. 11. (Color online) Density of states for the p electrons (dashed line) and d electrons (solid line) for $U=2$, $\Delta_0=1$, and $t_{pd}=0.9$. Left: DOS from analytically continued QMC data at $T=1/64$. Top panel has $\mu=0.829$ corresponding to a Mott insulating state ($\delta=0$). Middle panel has $\mu=0.529$ corresponding to small doping $\delta=n_{\rm tot}-3=-0.04$. Bottom panel has $\mu=0.329$ corresponding to high doping $\delta=-0.28$. The QMC data show the appearance of a broad quasiparticle peak (ZRP) at the Fermi level, in addition to the lower and upper Hubbard bands (LHB, UHB) at high energies. Right panels: comparison of DOS from ED-DMRG and QMC data (thick and thin lines, respectively) at the heavy doping $\delta=-0.28$. The ED-DMRG data are obtained using an environment of 30 sites.

tions can be stabilized. The true physical transition should occur where the free energy of the solutions cross. The precise determination of that line is beyond the scope of our present study and probably would require further refinement of the numerical techniques due to the very low energy scales involved.

One key point that provides further support to our results is the critical slowing down phenomenon observed in the QMC calculation at the phase boundaries of the coexistence region.[34,39] This phenomenon is characterized by an enhancement of the number of iterations required to achieve self-consistency and also by an enhancement of the statistical Monte Carlo fluctuations that reveal the shallowness of the energy landscape when two solutions merge. The root-mean-square deviation of the lowest frequency component of the d-electron Green's function is plotted in the inset of Fig. 9 as a function of μ for the low temperature $T=1/64$. As we approach the phase boundaries of the coexistence region, we can see that the root-mean-square deviation increases. Starting with an insulating solution, if we increase the chemical potential, the rms increases until we reach a critical value of μ, where the insulating solution disappears (open circles). Similarly, starting form a metallic solution at low doping, if we reduce the chemical potential, the rms grows until a critical value of μ, where the metallic solution disappears (open squares).

Evidently, the coexistence of solutions can also be observed from the behavior of other quantities, such as the double occupancy, or the low frequency part of the Green's functions. The latter is shown in Fig. 10 for both p- and d-electron components. These results support the claim that the MIT scenario for $\delta>0$ in the PAM is completely analogous to the one found in the Hubbard model investigations.[33–35]

2. Hole doping ($\delta<0$)

In the previous section we showed that upon particle doping, $\delta>0$, the Mott MIT in the PAM realizes the same physical scenario as the one observed in the single band Hubbard model. While in the latter the particle-hole symmetry implies an identical transition for $\delta<0$, we shall see that this is not the case in the PAM. A key point to appreciate is that we shall keep all model parameters fixed, with the obvious exception of the chemical potential, which controls the occupation. Therefore, if the chosen model parameters led, for $\delta>0$, to the identification of the PAM with the HM physics, then one may also expect that this would be the case for $\delta<0$ as well. Rather surprisingly this turns out not to be the case.[17] In this section we shall describe the main physical behavior of the model for the hole doping-driven MIT, and in the next we shall argue about the origin of this unexpected result.

We begin by showing the effect of hole doping in the DOS. In Fig. 11 we plot the change in the p and d components of the DOS as the system evolves from Mott insulator to a hole-doped metallic state (left panels, top to bottom). In the insulator state we observe that the chemical potential is located within the correlation gap, and the lower and upper Hubbard bands can be well appreciated. As we already discussed before, in this Mott insulator state the DOS at low frequencies has mostly d electron character, since the d orbital was initially located at the Fermi energy. Upon hole doping, the chemical potential moves within the lower Hubbard band. The metallization produces a wide and strong quasiparticle peak at the Fermi energy. At small doping, the low frequency part of the spectrum has a characteristic three peaks structure: the lower Hubbard band around $\omega\sim -0.4$, the quasiparticle peak that crosses the Fermi level, and the upper Hubbard band at $\omega\sim 0.8$ An interesting aspect to appreciate is that the quasiparticle peak has, as before, a larger d character, but, in addition, now it also has a substantial

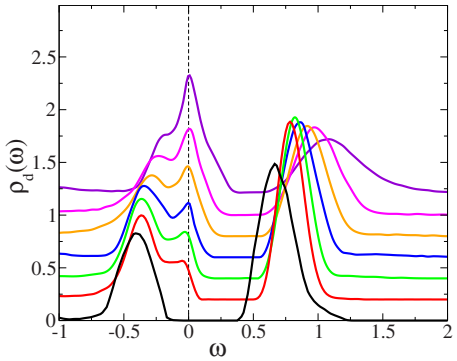

FIG. 12. (Color online) Density of states for d electrons for several values of hole doping from analytically continued QMC data at $U=2$, $\Delta_0=1$, $t_{pd}=0.9$, and $T=1/64$. From bottom to top, the hole doping is $\delta=0$, -0.01, -0.03, -0.04, -0.09, -0.15, and -0.28.

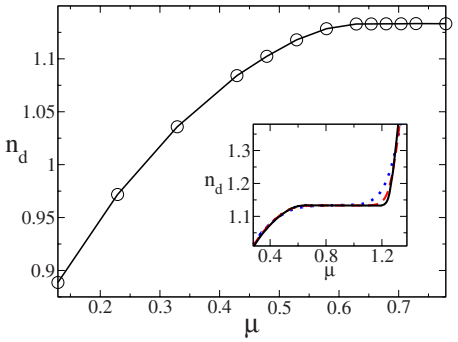

FIG. 13. (Color online) Partial occupation of the d electrons, n_d, as a function of the chemical potential μ at $U=2$, $\Delta_0=1$, and $t_{pd}=0.9$. Data are obtained from QMC calculations. Main panel has $T=1/128$. No trace of coexistent solutions is found. Inset has $T=1/16$, 1/32, and 1/64 (dotted, dashed, and full lines). Notice the strong temperature dependence on the particle-doped side of the transition (where only one branch of the hysteresis cycle at $T=1/64$ is shown) and the much less temperature dependence on the hole-doped side of the transition.

p-electron component. We shall see that this aspect will be consistent with the interpretation of the quasiparticle peak now emerging not from mere delocalization of d electrons as before, but from the delocalization of a composite object that involves a p-hole and a d-electron spin.

We can also observe a transfer of spectral weight, with an increase in the relative intensity of the lower Hubbard band plus quasiparticle, at the expense of a decrease in the upper Hubbard band. The structure that is seen below $\omega \approx -1.5$ corresponds to the fully filled band which remains with predominantly p-electron character. The results shown were obtained with high quality QMC data (at least 10^6 sweeps to reduce the statistical errors) and performed the analytic continuation to the real axis using the maximum entropy method.[24]

In the right panels of Fig. 11 we present a comparison of QMC and ED-DMRG results for the DOS at heavy doping $\delta=-0.28$. Similarly as before (cf. Fig. 7), the apparent multipeak substructures of the ED-DMRG results are not physical and only due to the discrete number of poles that result from a finite number of atomic sites in the auxiliary bath. Compared to the standard ED, this method produces much smoother spectra with greater detail due to the dramatic increase in the number of poles. However, as is also evident from the data, the discreteness due the finite-size representation of the bath remains a shortcoming of the method. The overall comparison of the two methods remains, nevertheless, very satisfactory and serves to illustrate their relative advantages and disadvantages.

To complete this study, we show in Fig. 12 the detailed evolution of the quasiparticle peak at the Fermi level plus the Hubbard bands as a function of doping. The data correspond to the d-electron density of states obtained from analytic continuation of QMC data.

The emergence of a quasiparticle peak at the Fermi energy for the hole-doped case may seem, at first sight, similar to the metallic state obtained from particle doping. However, this will not turn to be the case[17,41] and the physical origin of the two quasiparticle excitations will be shown to be qualitatively different. The reason for this unexpected asymmetry will be discussed in the next section.

In order to fully underpin the nature of the order of the hole-doped transition, we now look for hysteresis effects. Thus, as we did before, we continuously follow the solutions in parameter space. First, we start from the insulator and lower the chemical potential until we obtain a significantly doped metal; and then, we start from the metal and increase μ until we reach again the insulator. Neither our QMC numerical simulations nor the ED-DMRG studies showed any indication of hysteresis effects. The QMC data down to $T=1/128$ are shown in Fig. 13. Compared to the results for particle doping (inset), the present ones show a negligible temperature dependence. Thus, up to our current numerical capacity we have to conclude that the metal-insulator transition in the hole-doped case is of *second order*. As no evidence of coexistence has been found, neither in finite or zero-temperature calculations, we are led to the conclusion that the hole-doping-driven transition at $T=0$ is continuous, i.e., has a second-order character. Thus, it is qualitatively different from the particle-doped case, and, consequently, also qualitatively different from the Hubbard model scenario. Of course, we cannot rule out the eventual existence of tiny energy scales (which may modify our proposed scenario) which remain beyond the numerical precision of our methodology. This issue cannot be resolved nor by ED or ED-DMRG data due to the finite frequency cutoff set by the finite size of the clusters to diagonalize. Resolving this issue would probably require numerical renormalization group (NRG) study. However this is not fully clear since NRG method requires a good separation of energy scales, which is not the case here.

IV. DISCUSSION

Our results for the doping-driven MIT, which arise from either particle or hole doping of the Mott insulator, show a qualitative asymmetry, thus questioning the expected mapping of the PAM onto the Hubbard model. In this section we shall address in more detail this issue from the perspective of the physical nature of the two MIT taking place in the PAM.

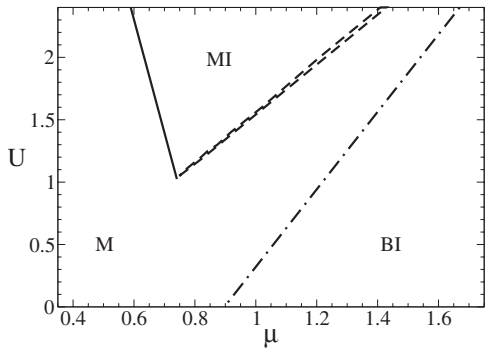

FIG. 14. Phase diagram of the PAM in the U-μ plane that maps the Mott insulator (MI) and its boundaries with the metallic state (M). The boundary between the metal and the band insulator (BI) at $n_{\mathrm{tot}}=4$ is also shown. The boundary lines are for $T=0$ ED star geometry calculations at $\Delta_0=1$ and $t_{pd}=0.9$. The dashed line denotes the region of the parameters where there is coexistence between two solutions, one metalliclike and the other one insulatinglike.

A. Phase diagram

To begin, we map out the phase diagram in U-μ parameter space to explore the respective ranges of the first- and the second-order transitions. Our results are summarized in Fig. 14, which was constructed using finite T quantum Monte Carlo and $T=0$ ED data. The latter were obtained using the "star-bath" geometry, which we found better suited[6,26] than the "chain-bath" geometry to study the possible coexistence between the metallic and the insulating regions.

The phase diagram in the U-μ plane shows a central V-shaped Mott insulator region with the correlated metallic phases for particle and hole doping, respectively, to the right and to the left. A threshold value for the strength of the interaction U (tip of the V-shape boundary) is required to obtain a Mott insulator state. This threshold depends on the value of the "band-structure" parameters Δ_0 and t_{pd}. This feature is analogous to the existence of critical value of the ratio U/D in the one-band Hubbard model.[6]

The central V-shaped Mott insulating region shows a remarkable asymmetry comparing the hole and the electron sides. In contrast, in the one-band Hubbard model, due to the particle-hole symmetry, the V-shape onset of the Mott insulator is symmetric with respect to the tip and behaves as $U_c \sim U_{c1} \pm 2\mu$, where U_{c1} is the value of the interaction at which the insulator disappears.[6] In the PAM, the transition line to the particle-doped side behaves as well like $U_c \sim \mathrm{const}+2\mu$. However, the transition line to the hole-doped metal is almost vertical.

We also mapped out the order of the transition along the boundary lines. Upon hole doping, both QMC calculations down to the low temperature $T=1/128$ and ED calculations at $T=0$ show no trace of coexistent solutions along all the transition line, indicating a second-order transition. On the other hand, upon particle doping, the dashed line in the phase diagram displays the region of the parameter space where, for sufficient low temperatures, an insulating state coexists with a metallic state. In fact within ED method at $T=0$ we find that the DMFT equations have two different solutions all along the transition line. Within QMC, and down to the low temperature $T=1/128$, we found a coexistence region only for a sufficiently large strength of the repulsive interaction U (approximately $U \approx 2$ for our specific choice of parameters). However, for smaller values of U, the phase boundary remains strongly dependent on temperature. This suggests that the temperature below which there is a coexistence between metallic and insulating state decreases rapidly approaching the tip of the V shape. This should be expected, since the two boundary lines, to holes and particle-doped metal, eventually merge at the tip. Similarly, we also expect the $T=0$ width of the coexistent region to become narrower as one approaches the tip of the V. However, obtaining detailed and precise numerical data there turned out to be beyond our methods' capabilities.

We note that at the Mott insulator state ($\delta=0$) the occupation of the conduction p electrons is almost saturated at $n_p=2-\nu$ (with $\nu \approx 0.1$). On the other hand, the occupation of the nondispersive d electrons which carry strong magnetic moments due to the on-site repulsion is close to 1, with $n_d=1+\nu$ (cf. Fig. 5). Therefore, there is only a small number $\sim \nu$ of p holes available to screen a number of order 1 of d magnetic moments. Therefore, a natural issue to consider is whether the physics associated to the "exhaustion problem" of Nozières[9,42,43] [see also related works on the Kondo lattice model[44,45] and on the PAM (Refs. 46–48)] may play a role in the different transitions at δ greater or smaller than 0.

An important point to realize is, however, that the exhaustion situation is even more extreme *on the particle side than on the hole-doped side*. In fact, while the number of d electrons remains always of order 1 on both sides, the number of available p holes is substantially smaller for $\delta>0$ with respect to the $\delta<0$ case. Nevertheless, the Hubbard-like first-order transition scenario takes place only on the particle-doped side. In other words, the PAM metal-insulator transition scenario is analogous to the one in the Hubbard model when the PAM is even deeper in the exhaustion limit ($\delta>0, n_p \approx 2$). This implies that while exhaustion should play a role, it is not obviously responsible for the failure of the mapping of the PAM onto the HM for $\delta<0$.

B. Nature of doped carriers

We now address the issue of the physical nature of the metallic states in this system. Although the low frequency parts of the DOS of both particle- and hole-doped metals have a similar three peaks structure with dominant d character, they realize physically different states. For instance, their charge compressibility has a very contrasting temperature dependence. In Fig. 15 we show the derivative of the total occupation with respect to the chemical potential, $\kappa = \partial n_{\mathrm{tot}}/\partial \mu$ (an observable proportional to the compressibility) as a function of doping. In the Mott insulator ($\delta=0$) κ is zero, indicating the incompressible Mott state. As expected, upon doping, k increases, indicating that the system becomes compressible. For small particle doping, the compressibility rapidly increases with the temperature, similarly as in the one-band Hubbard model case. Upon hole doping, κ is much less dependent on temperature.

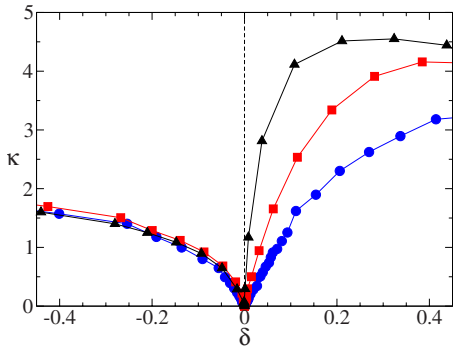

FIG. 15. (Color online) $\kappa=\partial n_{\mathrm{tot}}/\partial\mu$ as a function of doping δ, for several values of the temperatures $T=1/16,1/32,1/64$ (circles, squares, and triangles, respectively). Data are obtained from QMC calculations at $\Delta_0=1$, $t_{pd}=0.9$, and $U=2$. On the particle-doped side, we followed the metallic solution.

In the PAM the physics of the metallic states is usually discussed in terms of the screening between the p conduction electrons (or holes) and the magnetic moment of the local d electrons. In fact, at each lattice site a p and a d electron may form a local singlet, which is the underlying idea in the argument of Zhang and Rice[49] (ZR) in the context of high-temperature cuprate superconductors. However, if on the particle side of the Mott MIT we have argued that there are essentially no available holes, then the question is, what is screening the d moments so to produce a normal (but heavy) Fermi-liquid metal, analogous to the one in the doped Mott insulator in the Hubbard model?

The answer to this question is that, similarly to the one-band Hubbard model case, the d electrons are screening themselves. In fact, the local ZR singlet formation does not take place for $\delta>0$ simply because there are no holes available for screening. Nevertheless, despite the high filling of the p orbitals, the strong hybridization t_{pd} still allows for delocalization of the d electrons, through charge fluctuations across the p sites, with an effective amplitude $t_{\mathrm{eff}}\sim t_{pd}^2/\Delta$. The key physical point in this process is that since the p orbitals are almost full, they have a negligible local magnetic moment, so these charge fluctuations take place without significant magnetic p-d coupling. Therefore the magnetic phase coherence of the d electrons is preserved and, in consequence, a superexchange mechanism between neighboring d sites occurs. Thus, from the point of view of the d electrons, they have strong magnetic moments, they delocalize keeping their quantum mechanical phase through essentially nonmagnetic p sites, and therefore also experience antiferromagnetic correlations with nearest-neighbor d sites. These physical ingredients are evidently also realized for the carriers in the single band Hubbard model. Therefore we can now rationalize the underlying mechanism for the mapping of the PAM onto the one-band Hubbard model at $\delta>0$, cf. Fig. 16(a).

On the other hand, the situation is very different as the chemical potential is lowered to dope holes into the system. There, the number of available holes becomes more significant and they can lock with the robust d-magnetic moments to form local ZR singlets. However, when the d electrons of these singlets want to delocalize, i.e., hop to the neighboring

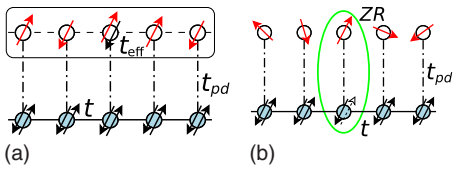

FIG. 16. (Color online) Schematic representation of the different types of carriers that occur upon either (a) particle ($\delta>0$) or (b) hole ($\delta<0$) doping of the Mott state.

sites and eventually form a quasiparticle band, they completely lose the information of their spin phase, thus the antiferromagnetic correlations between neighboring d do not build up. In consequence, Hubbard model like physics does not take place and the nature of both the MIT and the ensuing correlated metallic state becomes fundamentally different. That is the key physical reason why the mapping of the PAM with a one-band HM is no longer valid, cf. Fig. 16(b).

In order to substantiate the previous qualitative discussion, we show in Fig. 17 the d and p local moment formation as a function of doping for a large strength of the interaction U and for a value slightly above the tip. The local moment formation is defined as

$$\langle (m_\alpha^z)^2\rangle = \langle (n_{\alpha\uparrow}-n_{\alpha\downarrow})^2\rangle = n_\alpha - 2\langle n_{\alpha\uparrow}n_{\alpha\downarrow}\rangle, \qquad (17)$$

where $\alpha=p,d$. Notice that the difference between the particle occupation n and the moment directly measures the double occupancies of the sites. In the Mott insulator ($\delta=0$) the local moment of the d electrons, $\langle (m_d^z)^2\rangle$, is large because the d sites are predominantly singly occupied due to the effect of U. On the other hand, the p band is almost fully occupied, and thus the local moment of the p electron, $\langle (m_p^z)^2\rangle$, is significantly smaller. As one dopes the Mott insulator with particles or holes, the relative distribution of the local moments among both p and d sites is strikingly asymmetric. Upon particle doping, $\delta>0$, $\langle (m_p^z)^2\rangle$ becomes even smaller, since the occupation of the p band gets saturated. On the other hand, the d moment decreases more rapidly (and linearly) with the doping, since the charge fluctuations between the single occupied and double occupied d states increase.

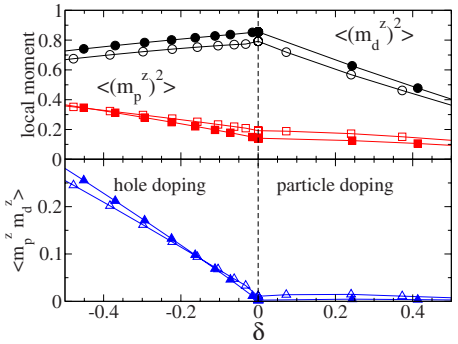

FIG. 17. (Color online) Top panel: $\langle (m_d^z)^2\rangle$ (circles) and $\langle (m_p^z)^2\rangle$ (squares) as a function of doping δ for $\Delta_0=1$, $t_{pd}=0.9$, $U=2$ (full symbols), and $U=1.2$ (open symbols). Bottom panel: $\langle m_p^z m_d^z\rangle$ as a function of doping δ for the same values of the parameters as in the main panel. The results are obtained with ED with star geometry.

Therefore these results support the view that for the particle-doped side of the transition the p sites are magnetically inert and, consequently, the d electrons screen themselves as they form a heavy mass metal. This heavy metal paramagnetic state is physically analogous to the one realized in the Hubbard model case. For the hole-doped metal, $\delta<0$, the p-electron local moment, $\langle(m_p^z)^2\rangle$, increases linearly with the doping because holes are mostly added to p sites. In contrast, the opposite behavior occurs for the d local moment, which slightly linearly decreases with hole doping. Thus, the increase in the magnetic character of p electrons is consistent with our argument for the formation of local singlets in the hole-doped case.

To fully underpin our hypothesis we compute the magnetic moment correlation between the d and p sites,

$$\langle m_p^z m_d^z\rangle = \langle (n_{d\uparrow} - n_{d\downarrow})(n_{p\uparrow} - n_{p\downarrow})\rangle. \tag{18}$$

The results are shown in the bottom panel of Fig. 17. They illustrate that in fact on the particle-doped side the magnetic correlations are negligible, however, on the hole doped side they increasingly grow as the chemical potential moves into the lower Hubbard band. The growth of the expectation value is commensurate with the increase in hole doping and signals that the doped p holes bind magnetically to the local d-electron magnetic moments. This represents the formation of the equivalent to Zhang-Rice singlets in the present model that only occurs at $\delta<0$.

C. Formation of Zhang-Rice-type singlets

The origin of the two different MIT scenarios and the resulting correlated metallic states can also be argued from an energetic point of view. The doping introduces new states inside the Mott gap Δ_M, which is renormalized by the hybridization t_{pd}. These states are a mixture of p and d states. An estimate of the energy gain of the Zhang-Rice singlet formation is

$$E_{ZR} \sim \nu(1-\nu)\frac{t_{pd}^2}{\Delta \pm \Delta_M}. \tag{19}$$

This results from the magnetic energy gain from the hopping of a p hole $(2-n_p=\nu)$ on a d site singly occupied $(1-\nu)$. We should compare the above binding energy with the delocalization energy of a d electron between two neighboring d sites, which is proportional to[50]

$$E_{SE} \sim (1-\nu)^2\frac{t_{pd}^4}{\Delta^2 U} = (1-\nu)^2\frac{t_{\text{eff}}^2}{U}. \tag{20}$$

This results from the virtual hopping of a d electron to its nearest-neighbor d site (i.e., through two p sites). *A priori* this gain is of order 1, since the d sites are approximatively all singly occupied and $1-\nu$ electrons participate in the superexchange process.[51] In fact, in the region of parameter we are investigating, the parameters t_{pd}, Δ, and U are of order 1. Therefore, the energy gain in the delocalization of a d electron [Eq. (20)] is of order $(1-\nu)^2$.

Upon particle doping, the energy gain of singlet formation (19) is of order $\nu(1-\nu)$, thus for small but finite ν, it is much smaller than the spin-exchange energy gain (20). Thus we can understand that for particle doping the spin-exchange energy gain dominates on the energy gain of singlet formation. This implies that the metallic state realized upon particle doping is due to the delocalization of mostly d electrons. Therefore the d electrons play the same role as the single type of carriers in the single band Hubbard model and produce a qualitatively similar MIT scenario.

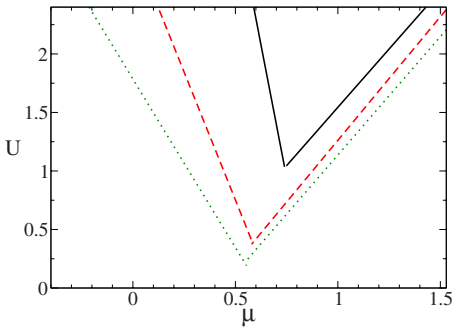

FIG. 18. (Color online) Phase diagram of the PAM in the U-μ plane that maps the Mott insulator and its boundaries with the metallic state. Data are for $t_{pd}=0.9$ and $\Delta_0=1,2,3$, i.e., $\epsilon_p=-1,-2,-3$ (solid, dashed, and dotted lines). Data are obtained with $T=0$ ED calculations.

On the other hand, upon hole doping, the energy gain of Zhang-Rice singlet formation can be substantial. In fact, in our region of parameters, Δ is of the same order of Δ_M, and the partial cancellation of the denominator in Eq. (19) explains that for a small but finite ν (which is controlled by the hybridization), the energy gain of singlet formation in the hole doped transition case dominates on the spin-exchange energy gain. Thus we can understand that, upon hole doping, the ensuing metallic state is due to the delocalization of these composite objects. The nature of this metallic state has been studied in detail in our recent work[41] where we found that it severely deviated from the Fermi-liquid paradigm. The physical reason is that the delocalized holes undergo a strong magnetic scattering from the local magnetic moments as they hop from site to site. Thus no coherent behavior for hole propagation is realized, at least down to very low temperature scales, leading to the observed non-Fermi-liquid character.

D. Restoring the mapping of PAM onto Hubbard model

We have shown that the new physics in the PAM with respect to the Hubbard model comes from the local coupling between the p and d electrons. Thus we expect that disfavoring this binding may restore the validity of the mapping on the hole-doped side of the MIT. To test this hypothesis, we lower the energy position of the p band, ϵ_p (i.e., we increase the charge-transfer energy Δ_0). We already noticed in Sec. III A that upon increasing the bare charge-transfer energy $\Delta_0=\epsilon_d-\epsilon_p$, the Mott gap approaches the bare value U and the mix-valence character of the electrons is in fact decreased.

In Fig. 18 we show the phase diagram in the plane U-μ for different values of the position of the p band. Upon in-

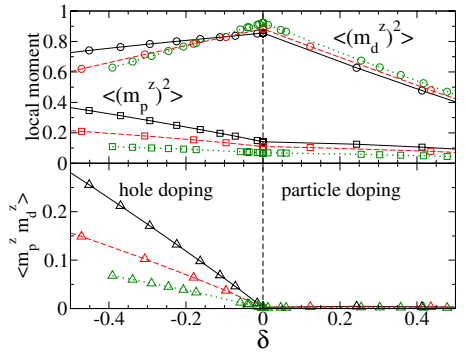

FIG. 19. (Color online) Top panel: $\langle(m_d^z)^2\rangle$ (circles) and $\langle(m_p^z)^2\rangle$ (squares) as a function of doping δ for $t_{pd}=0.9$ and U approximately two times larger than the threshold value to have a Mott gap (tip in the V shape of the phase diagram) and $\epsilon_p=-1,-2,-3$ (full, dashed, and dotted lines). Explicitly: $\epsilon_p=-1$ and $U=2$, $\epsilon_p=-2$ and $U=0.8$, $\epsilon_p=-3$ and $U=0.4$. Bottom panel: $\langle m_p^z m_d^z\rangle$ as a function of doping δ for the same values of the parameters as in the top panel. The results are obtained with $T=0$ ED star geometry calculations.

creasing Δ_0, the threshold value of U to obtain the Mott insulator region becomes smaller. This results from the fact that the interaction U is competing with a decreasing bandwidth $\sim t_{pd}^2/\Delta$. In addition, as expected, the V-shaped boundaries of the Mott insulator become more symmetric at larger Δ_0.

To verify whether the character of the transition can be modified on the hole-doped side, we observe the temperature behavior of the particle number, n. Upon increasing Δ_0, we find that n versus μ curves becomes more temperature dependent, which is a first indication of the possible realization of the Hubbard model scenario also in the hole-doped side. However, due to the reduction in the effective bandwidth $t_{\text{eff}}\sim t_{pd}^2/\Delta$, the temperature below which we may observe the hysteresis cycle in the n versus μ curves should be extremely low. With our current numerical capabilities we were only able to obtain evidence of a small hysteresis at $\Delta_0=3$.

To complete this study we also computed the local moment of p and d electrons upon increasing Δ_0. In Fig. 19 we plot the moments (top panel) and the magnetic binding between the p and d electrons (bottom panel) as a function of doping for several values of the position of the p band. In the Mott insulator ($\delta=0$), upon decreasing the position of the p band, $\langle(m_p^z)^2\rangle$ is decreased and $\langle(m_d^z)^2\rangle$ is increased. This is because the mix-valence character of the electrons is reduced, since the p band becomes essentially full with $n_p\rightarrow 2$ as $\epsilon_p\rightarrow-\infty$. Thus the doping has just a small effect on $\langle(m_p^z)^2\rangle$. On the other hand, upon hole doping, the d local moments decrease more rapidly when the p band is deep in energy. As a result, the magnetic correlation between the p and d electrons, $\langle m_p^z m_d^z\rangle$, shown in the bottom panel of Fig. 19, is expectedly punished by higher values of Δ_0. This is fully consistent with the mentioned recovery of the mapping of the PAM onto the Hubbard model. Therefore we can understand that for lowering in energy the position of the p band the mapping of the PAM onto the HM should hold.

V. CONCLUSIONS

In this paper, using DMFT, we considered the doping-driven Mott transitions of the periodic Anderson model when it is set in the Mott-Hubbard parameter regime. We discussed the transitions with respect to reference case of the well understood scenario realized in the single band Hubbard model.

In contrast to the latter, the PAM has a qualitatively different metal-insulator transition for particle or hole doping. Upon particle doping of the Mott insulator, the metallic state is reached through a first-order transition, which is analogous to that of the Hubbard model. However, upon hole doping the Mott insulator, there is a continuous (i.e., second-order) insulator-metal transition through a quantum critical line in the parameter space U-μ.

We argued that the hole-doped metal has delocalized Zhang-Rice singlets that fail to build substantial superexchange as compared to the Hubbard model (and particle-doped case). In fact, we discussed the qualitative differences between these two transitions showing that it is not due to the physics of the "exhaustion" but indeed is related to the magnetic interaction that develops between the two species of electrons in the model. Our results on the magnetic correlation between the d and the p electrons (see lower panel of Fig. 17) show that upon particle doping the p electrons permit the charge fluctuations and the delocalization of the d electrons without magnetic p-d coupling. On the hole-doped case, in contrast, the system favors the formation of singlet pairs p-d.

Upon increasing the charge-transfer energy, we could recover the mapping of the PAM to the Hubbard model for the hole-doped case. This signifies that a substantial mix-valence character was the key ingredient for the realization of the second-order transition in this model.

Our findings may be important looking at the present effort to apply DMFT calculation in regard to real materials.[52,53] Those studies usually carry the implicit assumption of the Hubbard model as the underlying low energy Hamiltonian of complex systems. Our work indicates that the Hubbard model scenario may be questionable when the hybridization of the correlated band with another band is high. In particular, our work is relevant for the analysis of the metal-insulator transitions of transition-metal oxides that usually have oxygen orbital mediating the delocalization of the d correlated electrons of the transition metal. Therefore the role of the oxygens band and their hybridization with the localized band should be explicitly considered in the investigation of the Mott transition.

ACKNOWLEDGMENTS

We acknowledge M. Gabay for useful discussions. A.A. acknowledges support from the European ESRT Marie-Curie program. G.S. and M.J.R. acknowledge support from the ECOS Sud-Secyt Program.

[1] N. F. Mott, *Metal Insulator Transitions* (Taylor & Francis, London, 1974).
[2] D. B. McWhan, A. Menth, J. P. Remeika, W. F. Brinkman, and T. M. Rice, Phys. Rev. B **7**, 1920 (1973).
[3] J. Hubbard, Proc. R. Soc. London, Ser. A **281**, 401 (1964).
[4] W. F. Brinkman and T. M. Rice, Phys. Rev. B **2**, 4302 (1970).
[5] W. Metzner and D. Vollhardt, Phys. Rev. Lett. **62**, 324 (1989).
[6] For a review, see A. Georges, G. Kotliar, W. Krauth, and M. J. Rozenberg, Rev. Mod. Phys. **68**, 13 (1996).
[7] M. J. Rozenberg, R. Chitra, and G. Kotliar, Phys. Rev. Lett. **83**, 3498 (1999).
[8] G. Kotliar, E. Lange, and M. J. Rozenberg, Phys. Rev. Lett. **84**, 5180 (2000).
[9] G. Kotliar, Eur. Phys. J. B **11**, 27 (1999).
[10] P. Limelette, A. Georges, D. Jérome, P. Wzietek, P. Metcalf, and J. M. Honig, Science **302**, 89 (2003).
[11] For a review, see M. Imada, A. Fujimori, and Y. Tokura, Rev. Mod. Phys. **70**, 1039 (1998).
[12] G. R. Stewart, Rev. Mod. Phys. **56**, 755 (1984).
[13] M. Jarrell, H. Akhlaghpour, and Th. Pruschke, Phys. Rev. Lett. **70**, 1670 (1993).
[14] M. J. Rozenberg, Phys. Rev. B **52**, 7369 (1995).
[15] M. Jarrell, Phys. Rev. B **51**, 7429 (1995).
[16] M. J. Rozenberg, G. Kotliar, and H. Kajueter, Phys. Rev. B **54**, 8452 (1996).
[17] G. Sordi, A. Amaricci, and M. J. Rozenberg, Phys. Rev. Lett. **99**, 196403 (2007).
[18] K. Held, C. Huscroft, R. T. Scalettar, and A. K. McMahan, Phys. Rev. Lett. **85**, 373 (2000).
[19] K. Held and R. Bulla, Eur. Phys. J. B **17**, 7 (2000).
[20] J. Zaanen, G. A. Sawatzky, and J. W. Allen, Phys. Rev. Lett. **55**, 418 (1985).
[21] A. Georges, G. Kotliar, and Q. Si, Int. J. Mod. Phys. B **6**, 705 (1992).
[22] H. O. Jeschke and G. Kotliar, Phys. Rev. B **71**, 085103 (2005).
[23] J. E. Hirsch and R. M. Fye, Phys. Rev. Lett. **56**, 2521 (1986).
[24] M. Jarrell and J. Gubernatis, Phys. Rep. **269**, 133 (1996).
[25] Q. Si, M. J. Rozenberg, G. Kotliar, and A. E. Ruckenstein, Phys. Rev. Lett. **72**, 2761 (1994).
[26] M. Caffarel and W. Krauth, Phys. Rev. Lett. **72**, 1545 (1994).
[27] M. J. Rozenberg, G. Moeller, and G. Kotliar, Mod. Phys. Lett. B **8**, 535 (1994).
[28] *Density Matrix Renormalization*, Lecture Notes in Physics Vol. 528, edited by I. Peschel *et al.* (Springer-Verlag, Berlin, 1999).
[29] S. R. White, Phys. Rev. Lett. **69**, 2863 (1992).
[30] U. Schollwöck, Rev. Mod. Phys. **77**, 259 (2005).
[31] D. J. Garcia, K. Hallberg, and M. J. Rozenberg, Phys. Rev. Lett. **93**, 246403 (2004).
[32] F. Gebhard, E. Jeckelmann, S. Mahlert, S. Nishimoto, and R. M. Noack, Eur. Phys. J. B **36**, 491 (2003).
[33] D. J. Garcia, E. Miranda, K. Hallberg, and M. J. Rozenberg, Phys. Rev. B **75**, 121102(R) (2007).
[34] G. Kotliar, S. Murthy, and M. J. Rozenberg, Phys. Rev. Lett. **89**, 046401 (2002).
[35] P. Werner and A. J. Millis, Phys. Rev. B **75**, 085108 (2007).
[36] Th. Pruschke, Z. Phys. B: Condens. Matter **81**, 319 (1990).
[37] M. J. Rozenberg, G. Kotliar, and X. Y. Zhang, Phys. Rev. B **49**, 10181 (1994).
[38] A. Georges and W. Krauth, Phys. Rev. B **48**, 7167 (1993).
[39] J. Joo and V. Oudovenko, Phys. Rev. B **64**, 193102 (2001).
[40] P. M. Chaikin and T. C. Lubensky, *Principles of Condensed Matter Physics* (Cambridge University Press, Cambridge, 1995).
[41] A. Amaricci, G. Sordi, and M. J. Rozenberg, Phys. Rev. Lett. **101**, 146403 (2008).
[42] P. Nozières, Ann. Phys. (Paris) **10**, 19 (1985).
[43] P. Nozières, Eur. Phys. J. B **6**, 447 (1998).
[44] S. Burdin, A. Georges, and D. R. Grempel, Phys. Rev. Lett. **85**, 1048 (2000).
[45] T. A. Costi and N. Manini, J. Low Temp. Phys. **126**, 835 (2002).
[46] A. N. Tahvildar-Zadeh, M. Jarrell, and J. K. Freericks, Phys. Rev. B **55**, R3332 (1997).
[47] A. N. Tahvildar-Zadeh, M. Jarrell, and J. K. Freericks, Phys. Rev. Lett. **80**, 5168 (1998).
[48] Th. Pruschke, R. Bulla, and M. Jarrell, Phys. Rev. B **61**, 12799 (2000).
[49] F. C. Zhang and T. M. Rice, Phys. Rev. B **37**, 3759 (1988).
[50] P. Fazekas, *Lecture Notes on Electron Correlation and Magnetism* (World Scientific, Singapore, 1999).
[51] P. W. Anderson, Phys. Rev. **79**, 350 (1950).
[52] G. Kotliar and D. Vollhardt, Phys. Today **57** (3), 53 (2004).
[53] G. Kotliar, S. Y. Savrasov, K. Haule, V. S. Oudovenko, O. Parcollet, and C. A. Marianetti, Rev. Mod. Phys. **78**, 865 (2006).